Unit Cell Approach to Full-Wave Analysis of Meander Delay Line Using FDTD Periodic Structure Modeling Method

Heeseok Lee and Joungho Kim

***Abstract*—Unit cell modeling is performed to determine the effect of electromagnetic coupling on the propagation characteristics of a meander delay line, which is widely used in printed circuit boards and packages. Since the design of a delay line must guarantee a several tens of picosecond timing margin in modern high-speed packages and board level interconnections, a penetrating understanding of the meander effect is essential. The propagation delay, the characteristic impedance, and the stop-band characteristic of the meander delay line have been carefully investigated based on a full-wave analysis using the finite-difference time-domain (FDTD) periodic structure modeling method. The periodicity of the meander line is utilized based on Floquet's theorem, resulting in a reduction of the computational domain in the FDTD simulation and providing a unit cell model of the meander line. The unit cell modeling of the meander delay line shows the effect of electromagnetic coupling in meander line structure on the reduction of the propagation delay. Also, an analysis based on the unit cell modeling was confirmed by time-domain reflection/transmission measurements. To investigate the effects of variation of substrate thickness (H) and trace width (W) generated during the manufacturing process, the propagation delay and the characteristic impedance were analyzed with different values of H and W. The unit cell modeling approach based on Floquet's propagation mode analysis produces a transmission line model of the meander delay line, which gives the dispersion relation and the characteristic impedance. This work should prove useful for high-speed digital circuit board designers.**

***Index Terms*—Delay line, finite-difference time-domain method, meander, periodic structure, signal integrity.**

I. Introduction

With the recent development of CPUs of over one gigahertz, the system bus speeds of modern computer systems have become increasingly fast. Accordingly, the timing budgets, related to the synchronization of the clock signal among the logic gates, must be much tighter. To avoid false operation of digital logic circuits, it is necessary to allow clock skew below adequate levels, necessitating the use of delay lines in package and board level interconnections. A popular solution for regular delay line design is the meander delay line, which has a regular, and thus delay-predictable, shape and compact design. To satisfy the tight clock skew requirement in the modern high-speed circuit board, the propagation delay through the meander line must be controlled within a range of just several tens of picoseconds. However, the electromagnetic coupling between the adjacent lines in the meander line structure causes a large amount of errors predicting the propagation delay along the meander line. Accordingly, an investigation of the full three-dimensional effects, including electromagnetic mutual coupling between the adjacent traces, in the meander line is essential to guarantee proper delay performance.

In this paper, the propagation characteristics of the meander delay line will be thoroughly examined based on a unit cell modeling approach using the finite-difference time-domain (FDTD) method [1]–[3]. Since the meander line structure includes numerous bends and coupled lines, a full-wave analysis is essential to consider the effects of the electromagnetic coupling and discontinuities in the meander line on signal integrity, including reflection, delay, dispersion, and distortion.

In previous studies, meander lines with a finite number of meander segments were analyzed to examine the propagation characteristic by using a full-wave analysis [4]–[7] or wave tracing analysis [8]. However, it is necessary to include a large number of meander segments to extract the transmission property of the meander line, which requires large computational resources such as memory and CPU time. Therefore, it has been suggested to utilize the periodic property based on Floquet's theorem [9] for study on the propagation characteristic of repeated complex structures such as meander delay lines [10]–[12].

Unit cell modeling based on Floquet's propagation mode analysis restricts the computational domain to a single unit cell of the repeated structure. Moreover, the unit cell approach gives a transmission line model of the meander delay line. In this work, the meander delay line is considered as a longitudinally periodic waveguide (LPW) based on Floquet's theorem. Consecutively, the FDTD periodic structure modeling method [1] is utilized to determine the propagation characteristics of the meandered delay lines widely used in printed circuit boards and of high-speed computer system packages. In particular, the effects of the mutual coupling between the adjacent traces in the meander line on propagation delay and characteristic impedance have been presented in detail. Also, the presented unit cell modeling of the meander delay line was confirmed by experimental data obtained by time-domain reflection (TDR)/time-domain transmission (TDT) measurements. In

Manuscript received October 30, 2001; revised March 27, 2002.

The authors are with the Terahertz Media and System Laboratory, Department of Electrical Engineering and Computer Science, Korea Advanced Institute of Science and Technology, Taejon 305-701, Korea (e-mail: heeslee@mail.kaist.ac.kr; joungho@ee.kaist.ac.kr; teralab@ee.kaist.ac.kr).

Digital Object Identifier 10.1109/TADVP.2002.803272

addition, the effects of dimensional feature variations generated during the manufacturing process have also been determined.

II. FDTD Method for Periodic Structure Modeling

Since a meander delay line is composed of repeated serpentine transmission lines, the meander line can be considered to be an LPW. Fig. 1 shows the wave function propagating through an arbitrary LPW. As presented in [1], the time-domain wave function, $F(x, y, z, t)$, propagating through an LPW is represented by the real part of the complex-number time-domain periodic function multiplied by the phase function, $e^{j\beta z}$, which is $F(x, y, z, t) = \int_0^{2\pi/d} \mathrm{Re}[F_p(x, y, z, t)e^{j\beta z}]d\beta$. Hence, $F_p(x, y, z, t)$ is periodic, which results in $F_p(x, y, z + d, t) = F_p(x, y, z, t)$. In this work, the FDTD computation was executed for the periodic complex function, $F_p(x, y, z, t)$, with the predetermined propagation constant β in the transformed β-domain. In this computational domain, the longitudinal spatial-derivative operator $\partial/\partial z$ must be replaced by $\partial/\partial z + j\beta$. The restriction of computational domain to a single period of an LPW by the longitudinal periodicity in the β-domain requires the computation of the time-domain complex function.

The presented FDTD method for periodic structure modeling calculates the transformed periodic electric field $\vec{E}(x, y, z, t)$ and magnetic field $\vec{H}(x, y, z, t)$ represented just in a single period ($z \in [0, d]$) with a predetermined propagation constant β and periodic boundary condition (PBC) given by $\vec{E}(x, y, z+d, t) = \vec{E}(x, y, z, t)$ and $\vec{H}(x, y, z + d, t) = \vec{H}(x, y, z, t)$. The update equations are given in (1) and (2) for the real part and the imaginary part of the H_x component, respectively

$$H^r_{x(p,\,q+0.5,\,r+0.5,\,n+0.5)} = \left[H^r_{x(p,q+0.5,r+0.5,n-0.5)} + \frac{\Delta t}{\mu} \times \left(\begin{array}{l} \dfrac{\beta}{2}\left(E^i_{y(p,q+0.5,r+1,n)} + E^i_{y(p,q+0.5,r,n)}\right) \\ -\dfrac{E^r_{z(p,q+1,r+0.5,n)} - E^r_{z(p,q,r+0.5,n)}}{\Delta y} \\ +\dfrac{E^r_{y(p,q+0.5,r+1,n)} - E^r_{y(p,q+0.5,r,n)}}{\Delta z} \end{array} \right) \right] \tag{1}$$

$$H^i_{x(p,q+0.5,r+0.5,n+0.5)} = \left[H^i_{x(p,q+0.5,r+0.5,n-0.5)} - \frac{\Delta t}{\mu} \times \left(\begin{array}{l} \dfrac{\beta}{2}\left(E^r_{y(p,q+0.5,r+1,n)} + E^r_{y(p,q+0.5,r,n)}\right) \\ +\dfrac{E^i_{z(p,q+1,r+0.5,n)} - E^i_{z(p,q,r+0.5,n)}}{\Delta y} \\ -\dfrac{E^i_{y(p,q+0.5,r+1,n)} - E^i_{y(p,q+0.5,r,n)}}{\Delta z} \end{array} \right) \right]. \tag{2}$$

In (1) and (2), Δt is the time step and Δy and Δz are the spatial mesh sizes along the y-axis and z-axis, respectively. $H^r_{x(p,\,q,\,r,\,n)}$ represents the real part of $H_x(p\Delta x, q\Delta y, r\Delta z, n\Delta t)$, where p, q, r, and n are integers for the index. The finite-difference equations for the remaining ten components can be derived in the same manner.

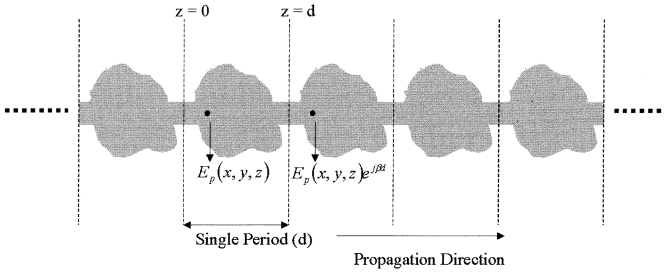

Fig. 1. Arbitrary periodic waveguiding structure with longitudinal periodicity. The longitudinal direction is parallel to Z-axis. The wave function for the guided wave in a longitudinally periodic waveguide can be represented by the periodic function multiplied by the phase function $\exp(j\beta z)$.

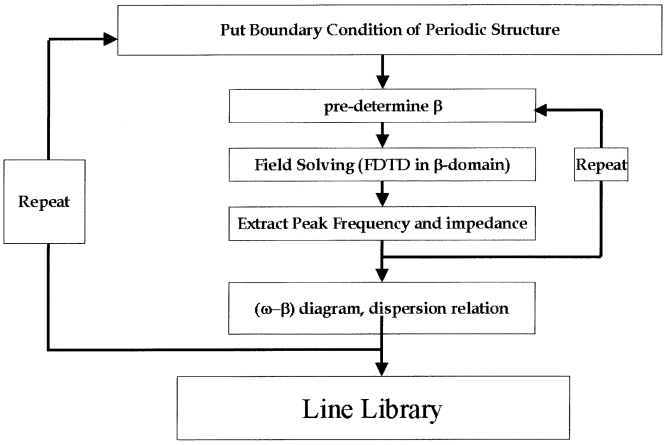

Fig. 2. Routine for dispersion analysis using FDTD method.

With a predetermined propagation constant, β, a FDTD simulation is performed to obtain the impulse response. The peak frequencies of the modes corresponding to the predetermined propagation constant β used in each FDTD run are obtained by a fast Fourier transform (FFT) of the calculated impulse response. Fig. 2 shows the flow chart for the dispersion analysis of the LPW by the FDTD modeling. The FDTD simulation and the FFT of the impulse response for each β give the dispersion diagram of a LPW, which can be found in Figs. 4, 6, 7, and 12. As is well known, since the dispersion diagram of a LPW is periodic, the FDTD computation is required just within $0 < \beta < 2\pi/d$. The presented periodic structure modeling approach saves computational costs for full-wave simulations of repeated structures such as the presented meander delay line. Furthermore, the available computer memory resource can be concentrated on the FDTD computation of unit cell to enhance the resolution of the numerical spatial mesh based on the presented unit cell approach, promising accurate numerical modeling.

III. Unit Cell Modeling of Meander Delay Line

As shown in Fig. 3, the meander line can be considered to be a repeated structure of a unit cell. The unit cell of the meander line is defined by the periodic boundary given in Fig. 3. Using the presented FDTD method based on Floquet's theorem, the transmission characteristics of the meander line are analyzed, in

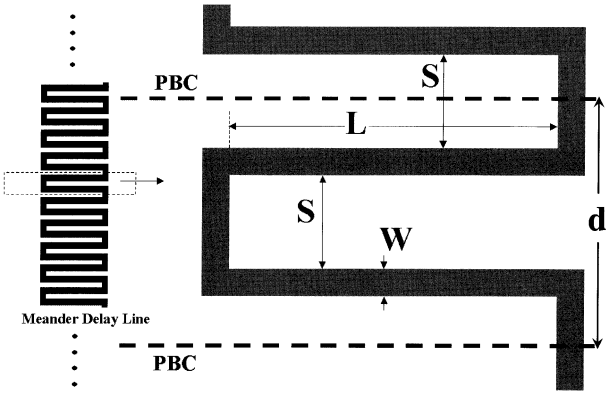

Fig. 3. Schematic of meander delay line. Periodic boundary condition (PBC) inherited from Floquet's theorem reduces the computational domain to a single unit cell of the meander delay line. In this study, a stripline configuration is used. The thickness of the substrate is 0.9 mm. The stripline trace is 0.3 mm ($=H$) over the bottom ground plane. The width of the trace (W) is 0.2 mm. L is 6 mm. S is selected to be 0.2 mm, 0.4 mm, 0.6 mm, 0.8 mm, and 1.0 mm for T1, T2, T3, T4, and T5, respectively.

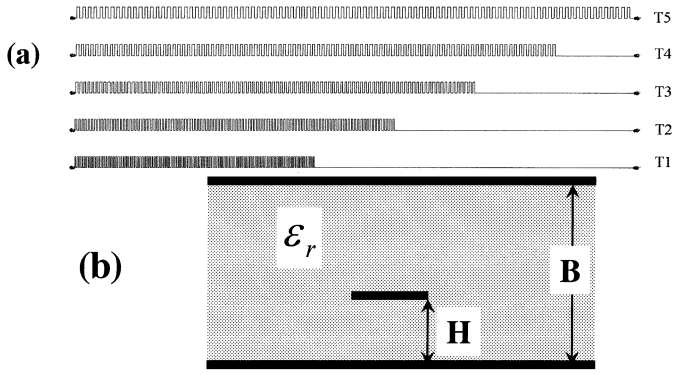

Fig. 5. (a) Meander line trace patterns, which have 100 meander units with various values of S. These traces are prepared for TDR/TDT measurement experiment. A FR-4 dielectric substrate was used. The values of S are 0.2 mm, 0.4 mm, 0.6 mm, 0.8 mm, and 1.0 mm for T1, T2, T3, T4, and T5, respectively. The physical lengths of the traces are 1480 mm. (b) Cross section view of the stripline used in this study. The thickness of the substrate is 0.9 mm ($=B$). The distance between the signal trace and the bottom ground plane is 0.3 mm ($=H$).

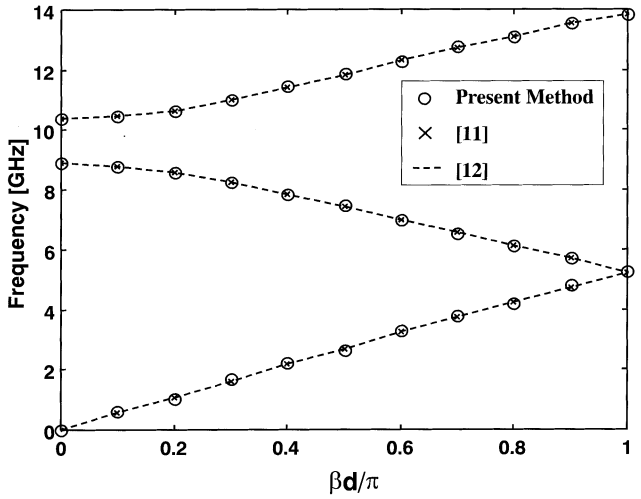

Fig. 4. Dispersion diagram of the meander microstrip line. This is presented to verify the accuracy of the presented method by comparison with the published data given in [11] and [12]. The geometrical features used in this simulation were the same as those employed in [11] and [12]. ($W = 2.37$ mm, $S = W$, $d = 4W$, $L = 2W$).

terms of the propagation delay and the characteristic impedance. The effect of the electromagnetic coupling between the adjacent traces in the meander delay line is also investigated in a single period with the longitudinally periodic boundary condition (PBC).

First, to verify the accuracy of the presented method, the dispersion diagram of the meander microstrip line given in [11] and [12] was obtained and compared. As shown in Fig. 4, the calculated results obtained by the presented FDTD method match well with [11] and [12], demonstrating the validity of the presented method.

A. Effect of Electromagnetic Coupling on Propagation Delay

For high-speed circuit board designers, one of the important properties of the meander delay line is propagation delay. To accurately characterize the transmission characteristic related to the propagation delay generated by the meander delay line, the effect of the electromagnetic coupling must be carefully considered. First, the dispersion diagram of the meander delay line is obtained by using the presented FDTD method with varying distances between the adjacent traces in the meander line (S given in Fig. 3). The width (W) of the signal trace is 0.2 mm and the value of L (indicated at Fig. 3) is 6 mm. The feature of the meander striplines, designated as T1, T2, T3, T4, and T5, are the different values of S, 0.2 mm ($=W$), 0.4 mm ($=2W$), 0.6 mm ($=3W$), 0.8 mm ($=4W$), and 1.0 mm ($=5W$), respectively. A cross-section of the stripline configuration used in this study is presented in Fig. 5(b), where $H = 0.3$ mm, $B = 0.9$ mm, and $\varepsilon_r = 4.5$. The computational domain was discretized by a $(0.05\text{ mm})^3$ cubic cell to resolve the 0.2 mm wide signal trace with a factor of 4. A 50 fs time step size was used for the numerical stability. The stripline trace was placed 0.3 mm over the bottom ground plane. In the FDTD simulation, the traces and the ground planes are considered to be perfect conductors with zero thickness.

The calculated dispersion diagrams are given in Figs. 6 and 7. The dispersion diagram shown in Fig. 6(a) is the dispersion relation of the meander delay line, indicated by "T1," whose geometric feature is $S = W$. Fig. 6(b) shows the first stop-band of each meander line, which separates the first branch and the second one in the dispersion diagram. The stop-bands of the given meander delay lines are placed around 10 GHz. If the signal propagating through the meander line has a frequency spectrum larger than the stop-band frequency, the transmitted waveform suffers from band rejection, resulting in ringing of the transmitted time-domain waveform. To prevent severe signal distortion, the stop-band of the meander line must be kept larger than the maximum frequency of the propagating signal. The stop-band is determined by the length of the coupled line, indicated by L as shown in Fig. 3. Hence, L is the geometric parameter to determine the high-frequency limit of the meander delay line. The stop-band frequency can be roughly calculated by a simple arithmetic formula based on the simulated results, $3.0 \times 10^8/((2L+S)\sqrt{\varepsilon_r})$. In addition, it is observed that as the

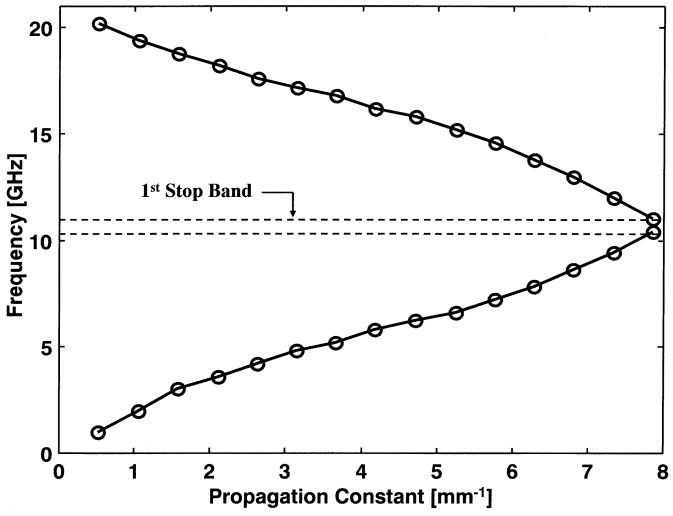

(a)

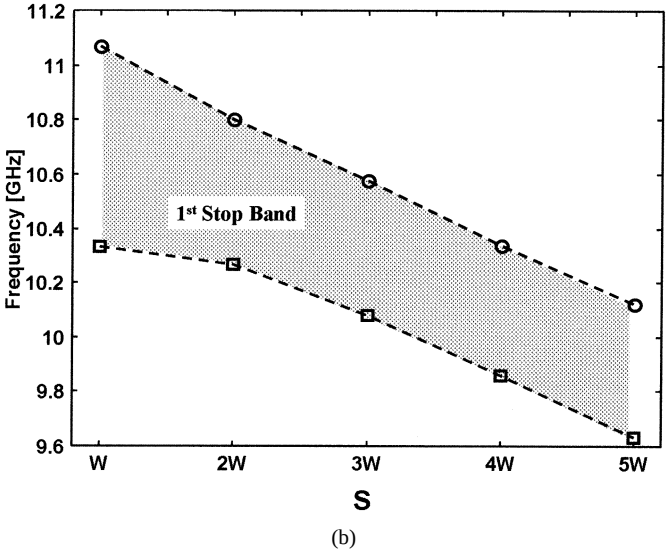

(b)

Fig. 6. (a) Dispersion diagram for the meander delay line ($S = 0.2$ mm, T1). These curves are obtained by dispersion analysis using the presented FDTD simulation based on Floquet's mode analysis. In this figure, the first and second branches are given. The stop-band (10.33 GHz $< f <$ 11.07 GHz) is indicated by the dotted lines. (b) The stop-bands of the five patterns (T1–T5). These are also calculated results obtained by FDTD simulation.

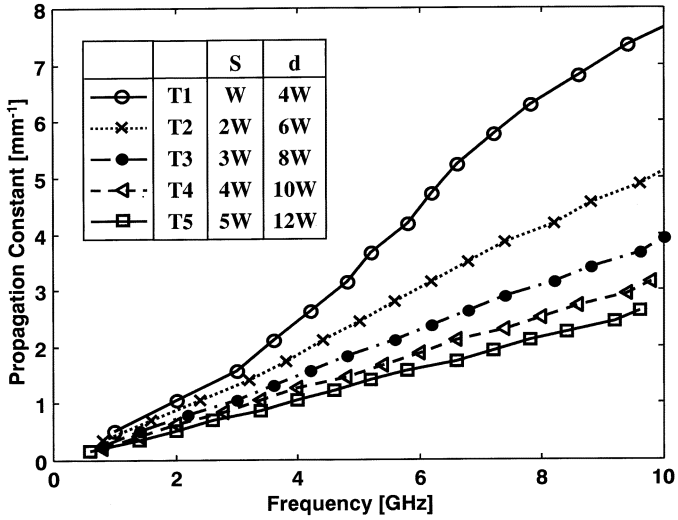

Fig. 7. Dispersion relation for five meander delay lines (T1–T5). These curves are obtained by dispersion analysis using the presented FDTD simulation. They are the first branches of the dispersion diagram of the each meander pattern.

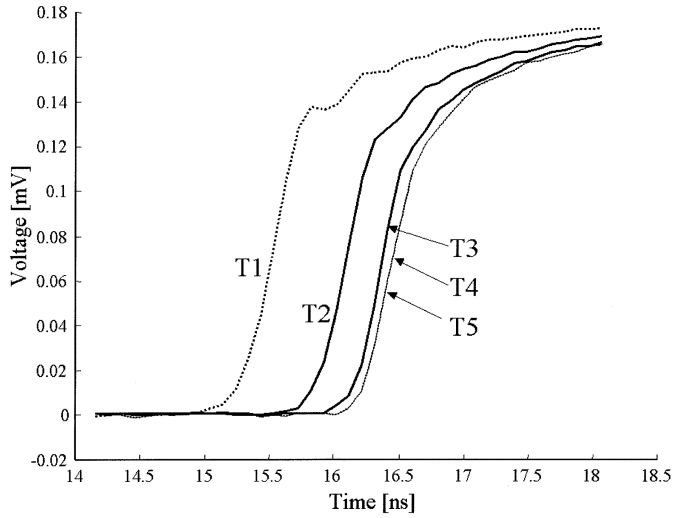

Fig. 8. Time-domain waveforms measured by TDR/TDT equipment at rising period.

adjacent traces become closer, the stop-band becomes slightly wider.

Since the cutoff frequency of the trapezoidal wave with a rising time more than 30 ps is less than 10 GHz, the first branch of the dispersion diagram is necessary for signal integrity analysis in modern high-speed circuit board design. Fig. 7 presents the first branches of each of the meander delay line patterns, designated as T1–T5. As predicted, the meander line designed with a small S value (given in Fig. 3) is the slowest delay line, which means that it is the most efficient meander pattern in terms of possession of circuit board area. However, the electromagnetic coupling in the T1 meander line may have a significant effect on the propagation delay. Since the propagation delay through a meander delay line must be predictable, T1 ($S = W$) may not be employable in spite of its superiority in terms of circuit area efficiency. Hence, the effect of the mutual coupling in the meander line must be carefully investigated.

Together with the simulation result obtained by the FDTD unit-cell modeling, a series of meander striplines are analyzed by TDR/TDT measurements. The test vehicles for the meander delay line were prepared as shown in Fig. 5(a). The line was fabricated with a 0.9 mm thick FR-4 substrate with the stripline configuration shown in Fig. 5(b). Each meander trace pattern has 100 unit cells of meander line and the physical lengths of the T1–T5 traces are all 1480 mm. If there is no electromagnetic coupling between the adjacent meanders, the propagation delay for all five traces must be identical. However, as can be seen in Fig. 8, the flight time (T) is given by $T_{T1} < T_{T2} < T_{T3} < T_{T4} \approx T_{T5}$. It is observed that the electromagnetic coupling reduces the electrical length of the meander delay line. In short, from the experimental results obtained by TDT measurement, when S is larger than $4W$, the effect of the electromagnetic coupling in a given meander delay line on the propagation delay is not significant.

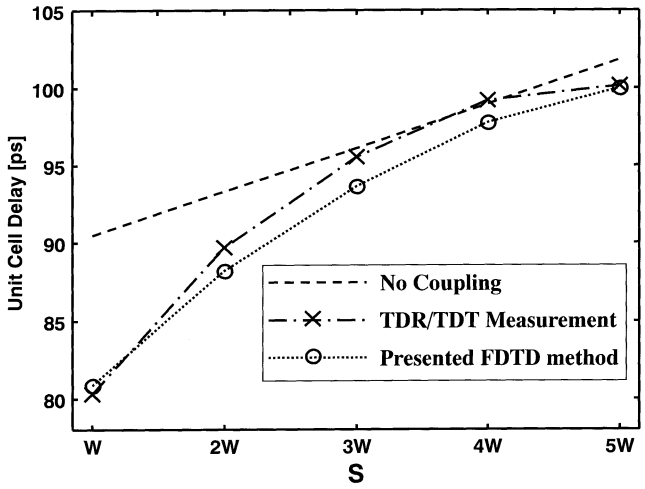

Fig. 9. Unit cell delay presented in y-axis indicates the propagation delay time through a single unit cell of the meander line. They are calculated from the TDR/TDT measurement data (indicated by X) and obtained from the FDTD simulation results (indicated by O). To demonstrate the electromagnetic coupling effect on the flight time in the meander delay line, the unit cell delay estimated without mutual coupling effect is also presented, which is indicated by "No Coupling."

From the TDR/TDT measured data, the propagation delay through a single meander cell can be calculated. The velocity of the straight stripline was measured by two straight striplines of different lengths. From the difference of the flight time, the velocity of the stripline is calculated to be 1.4085×10^8 m/s, from which the measured relative dielectric constant of the substrate is about 4.53. Using this measured velocity of the straight stripline, the propagation delay through a unit cell (unit cell delay) of the meander delay line is calculated.

To compare the measured result and the simulation, the unit cell delay is also calculated based on the presented FDTD modeling. Since the rising time of the trapezoidal wave generated by the TDR/TDT equipment used in this work is about 80 ps, the cutoff frequency is about 4 GHz. Utilizing the dispersion relation presented in Fig. 7, the unit cell delay has been obtained. Fig. 9 shows the unit cell delay of each meander line structure. In order to demonstrate the effect of the electromagnetic coupling on the propagation delay, the unit cell delay estimated with the assumption that there is no coupling effect in the meander delay line is also given in Fig. 9. If there is no effect from the electromagnetic coupling in the meander line, the relation between the unit cell delay and the value of $\boldsymbol{S}$ (separation between the adjacent traces) must be linear, as shown by the dotted line indicated by "No Coupling" in Fig. 9. However, in a real situation, the electromagnetic coupling causes a significant reduction in the electrical length of the meander delay line. To summarize, the propagation delays through each single meander structure are presented in Fig. 9, which compares the TDR/TDT measurement and the FDTD numerical simulation. As can be seen, the tendency of the unit cell delay matches well. The obtained unit-cell modeling provides a very useful scalable solution for meander delay line design. In other words, the propagation delay for the meander delay line including any number of meander units can be calculated based on the presented modeling method.

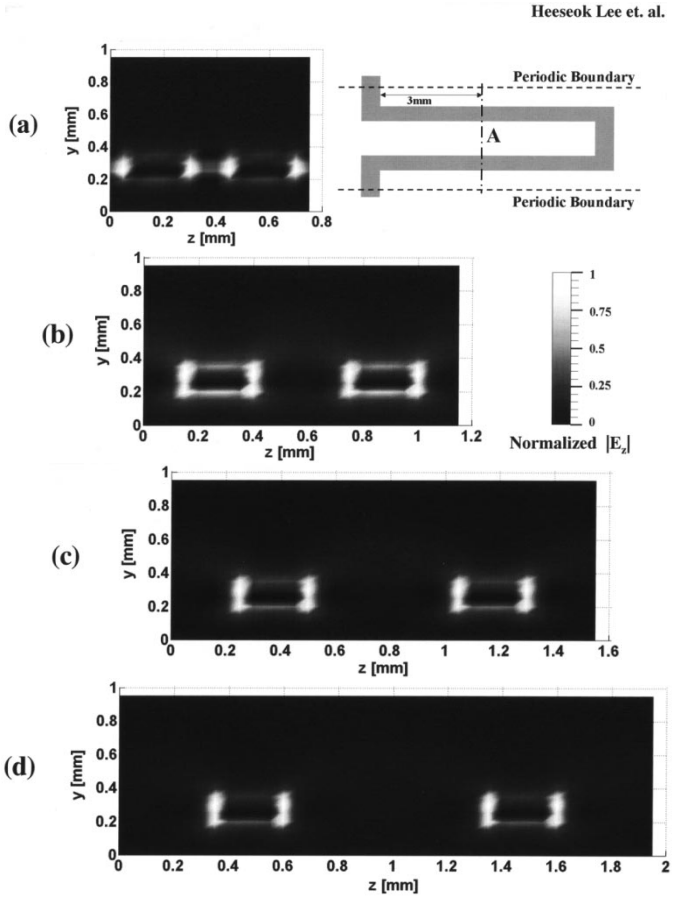

Fig. 10. Electric field ($|\boldsymbol{E_Z}|$) distribution at 5 GHz on the y–z plane crossing the line A, which is indicated in (a). The distributions are calculated by FDTD simulation with longitudinally periodic boundary. The distances between the adjacent parallel lines are 0.2 mm (T1), 0.4 mm (T2), 0.6 mm (T3), and 0.8 mm (T4) for (a)–(d), respectively. The intensity of the electric field $|\boldsymbol{E_Z}|$ is normalized. In (a), the coupling between the adjacent lines seems to be very strong, which is believed to cause a reduction in the propagation delay.

Although all coupling phenomena and discontinuity effects that occur in the meander line are considered in the presented numerical modeling process, the electromagnetic mutual coupling between the adjacent parallel lines is believed to have the most dominant effect on the propagation delay. Fig. 10 shows the longitudinal electric field distribution, $|\boldsymbol{E_Z}(\boldsymbol{y},\boldsymbol{z})|$, between adjacent parallel lines in a unit cell, demonstrating the coupling strength between the adjacent lines. The strong mutual coupling between the adjacent lines in the meander line structure given by the T1 ($\boldsymbol{S} = \boldsymbol{W}$) trace pattern can be observed in the electric field distribution shown in Fig. 10(a). The significant reduction of the propagation delay in the trace pattern T1 is considered to be due to the strong electromagnetic coupling between the adjacent lines (see Fig. 11).

B. Characteristic Impedance of Meander Delay Line

In addition to the propagation delay, the characteristic impedance is also an important propagation characteristic of the transmission line element. In this section, the effect of the electromagnetic coupling in the meander line on the characteristic impedance has been investigated. Generally,

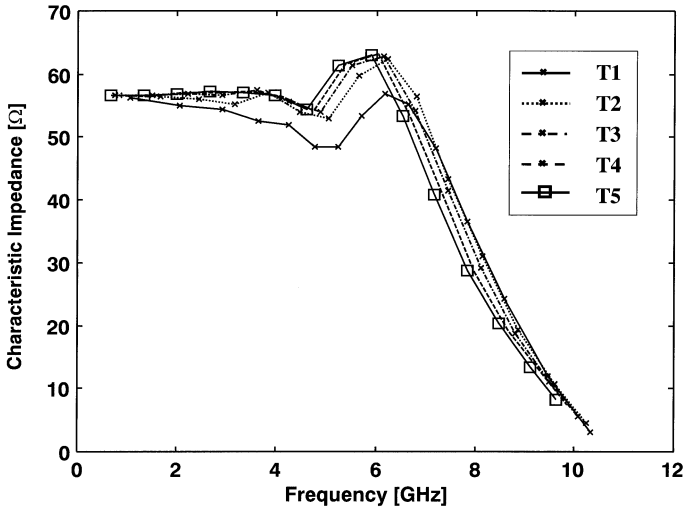

Fig. 11. Characteristic impedances of T1–T5. The characteristic impedance is defined at the plane indicated by PBC in Fig. 3. In other words, the reference terminal of the meander line is the end of the unit cell.

the characteristic impedance of the periodic structure is frequency-dependent and is defined at the reference terminal in the unit cell [9]. In this work, the characteristic impedance is defined at the plane indicated by PBC in Fig. 3. In other words, the reference terminal of the meander line is defined to be the end of the unit cell. It is observed that as the frequency closes to the stop band, the characteristic impedance of the meander delay line changes and decreases. Finally, the characteristic impedance approaches zero near the bandgap frequency, as presented in Fig. 6(b). This frequency-dependent property of the characteristic impedance of longitudinally periodic structures has been previously reported in [13].

As discussed in the previous section, since the propagation characteristic near the stop-band of the meander line is poor, the cut-off frequency of the signal transmitted through the meander line must be less than the stop-band frequency of the meander delay line. While the stop-band is near 10 GHz, the change of the characteristic impedance begins around 5 GHz. Therefore, the stop-band frequency limit of the given meander delay line must be carefully designed to be larger than the cutoff frequency of the signal to satisfy the tight signal integrity requirement. While the characteristic impedances of T3–T5 are nearly constant below 4 GHz, those of T1 and T2 slightly decrease and fluctuate as frequency increases. While the characteristic impedance of T4 is about 55 Ω and 54 Ω at 1 GHz and 4.5 GHz, respectively, that of T1 at 1 GHz and 4.5 GHz is about 55 Ω and 47 Ω, respectively. As given, the strong mutual coupling in the meander delay line causes the frequency-dependent characteristic impedance. In order to utilize the meander delay line as a straight line in a circuit board, the meander segments are separated at a distance great enough to ignore the effect of electromagnetic coupling.

C. Effect of Variation in Substrate Thickness and Trace Width on Propagation Delay and Characteristic Impedance

In manufacturing processes, the thickness of the dielectric substrate, the width of the signal trace, and the dielectric constant of the substrate may often not match the designed value

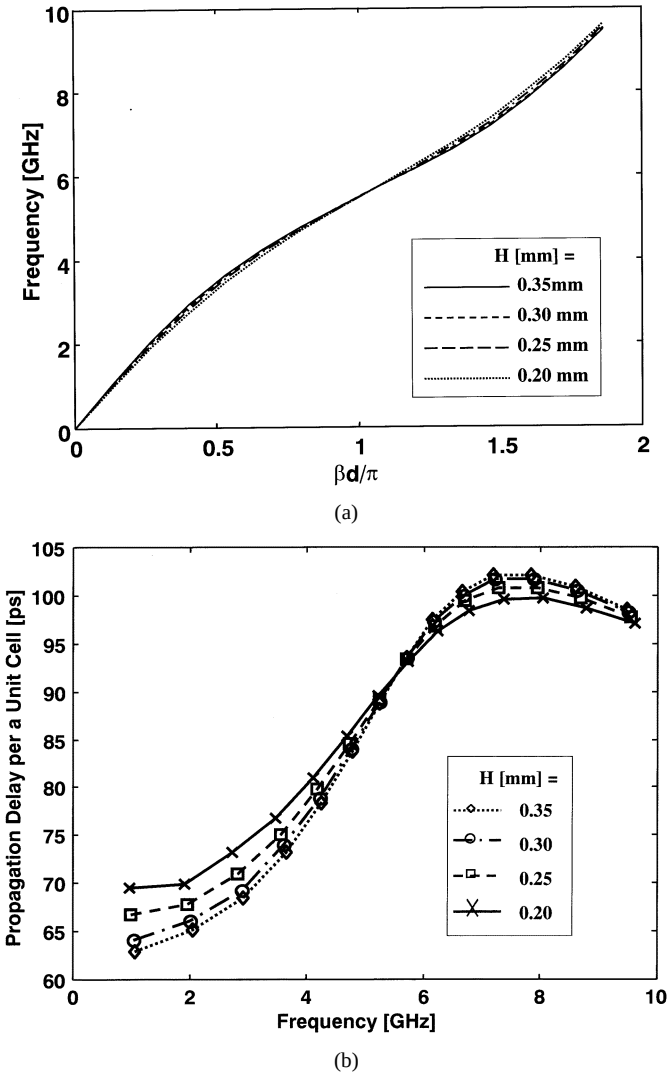

Fig. 12. (a) Dispersion diagram of the meander delay line with four different values of $\boldsymbol{H}$, $\boldsymbol{W}$ = 0.2 mm, $\boldsymbol{S} = \boldsymbol{W}$, and $\boldsymbol{d} = 4\boldsymbol{W}$. (b) Frequency-dependent propagation delay time per unit cell, which is calculated based on the dispersion relation presented in (a). The increase of separation between the signal traces and the bottom ground plane causes a reduction in the propagation delay below 5 GHz.

exactly. While the effect of the dielectric constant on the propagation characteristic is linear and predictable without additional full wave analysis, variation of the geometrical features causes a change in the electromagnetic coupling in the meander line. Hence, the effect of the manufacturing variation in substrate thickness and trace width on the propagation delay and the characteristic impedance of the meander delay line are carefully examined based on the presented unit cell modeling method.

Fig. 12 presents the dispersion property of the meander delay line, whose feature is $\boldsymbol{S} = \boldsymbol{W}$, with respect to four different values of substrate thickness ($\boldsymbol{H}$). The first branch of the dispersion diagram and the frequency-dependent unit cell delay are given in Fig. 12(a) and Fig. 12(b), respectively. The frequency-dependent unit cell delay was calculated by $\tau_{delay}(f) = \beta(f)d/2\pi f$ using the frequency-dependent phase velocity obtained by FDTD method. Below 5 GHz, while the increase of the value of $\boldsymbol{H}$ reduces propagation delay, the closer distance between the signal trace and the bottom ground plane provides

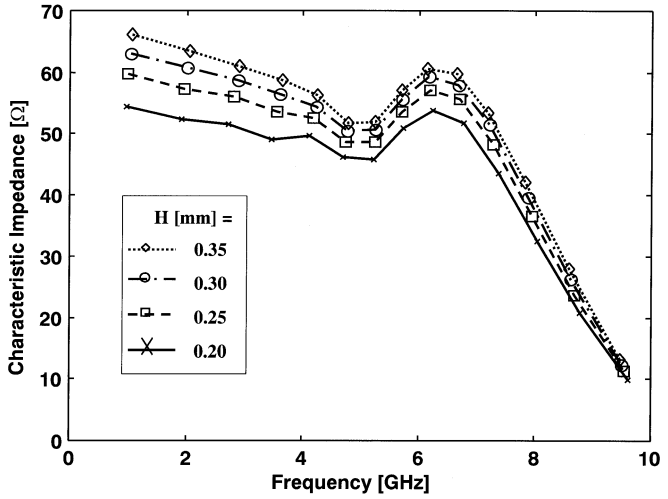

Fig. 13. Variation of characteristic impedance with respect to four different values of H. The geometric features of the meander line used in this work are $W = 0.2$ mm, $S = W$, and $d = 4W$.

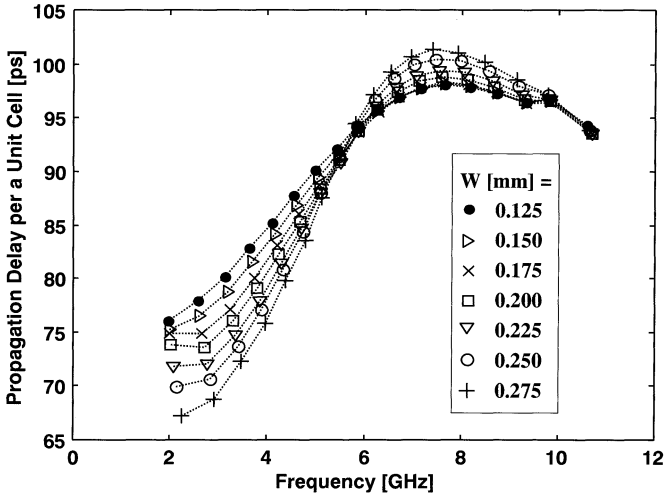

Fig. 14. Frequency-dependent propagation delay time per unit cell with respect to different values of W. In the FDTD simulation, the period of the meander delay line was fixed at $d = 4W$. Changing the width of the signal trace, the distance between the adjacent signal traces is reduced. The decrease of the separation between the adjacent traces causes a reduction in the propagation delay below 5 GHz. ($d = 4W$, $S = 0.4$ mm $- W$.)

larger unit cell delay. Since the smaller value of H makes field confinement between the signal trace and the bottom ground plane tighter, the effect of the mutual coupling between the adjacent traces is reduced. However, this tendency of the unit cell delay is reversed over 6 GHz. Since poor characteristic impedance performance of a meander delay line over 6 GHz cannot guarantee a high quality transmitted signal, transmission of the signal component near the stop-band frequency in the meander line is not discussed in this paper in detail. The characteristic impedances with respect to the four different values of H are given in Fig. 13. It is observed that the effect of the substrate thickness variation on the characteristic impedance is nearly similar to the characteristic of a straight stripline. As is well known, the small value of W/H gives high impedance.

The variation of trace width is determined by lithography technology and an etching process (or deposition process). In this study, the effect of the signal trace width on the propagation delay has been determined in the range of 0.2 mm$\pm$0.075 mm with the same geometrical values of L and d (given in Fig. 3). In this work, the half size of the spatial mesh used in the previous FDTD simulation was used to achieve 0.025 mm spatial resolution. Fig. 14 presents the frequency-dependent unit cell delays with respect to seven different values of trace width (W). In this work, the period of the meander delay line (d) was fixed at $4W$. Below 5 GHz, while the propagation delay for the largest value of the trace width ($W = 0.275$ mm) is the smallest, the meander line with $W = 0.125$ mm gives the largest propagation delay. This phenomenon can also be explained by the electromagnetic coupling between the adjacent signal traces. Since the value of S for the given seven meander line patterns is $S = (0.4$ mm $- W)$, the meander line with $W = 0.275$ mm has smallest S, which increases the electromagnetic coupling between the adjacent traces. As discussed in the previous sections, the electromagnetic coupling causes a reduction in the propagation delay.

IV. Conclusions

To control the propagation delay of signal transmission, the meander line is a very popular delay line structure in package and board level interconnections. For precise and appropriate design of the meander delay line, a more profound understanding of the electromagnetic coupling between the adjacent line segments of meander delay line is essential. In this paper, the FDTD method was utilized to analyze Floquet's propagation mode of the meander delay line. The periodic boundary based on Floquet's theorem results in a reduction of the computational domain in the FDTD modeling. By utilizing the presented method, unit cell modeling of the meander delay line has been performed for determination of the propagation characteristic of the meander delay line.

To verify the analysis of the meander delay line based on the presented unit cell modeling, the experimental result obtained by the TDR/TDT measurement has been presented, which shows the coupling effect of the adjacent lines on the reduction of the propagation delay. Furthermore, stop-band characteristic and the characteristic impedance of the meander line have also been discussed. To ignore the effect of the coupling on the propagation delay and the impedance, the adjacent traces must be separated at an adequate distance. To promise the best quality of the transmitted signal, the stop-band frequency of the meander line must be larger than the cut-off frequency of signal. The value of L given in Fig. 3 determines the bandgap frequency of the meander delay line.

To determine the manufacturing tolerance, the effects of the variation of the substrate thickness and the trace width have also been investigated, in terms of the propagation delay and the characteristic impedance. Conclusively, the propagation characteristic of the meander line has been presented based on a full-wave analysis utilizing FDTD periodic structure modeling. The presented set of the dispersion relations, $\beta(f)$, and the characteristic impedance, $Z_0(f)$, for a unit cell give a simple transmission line model of the meander line. Hence, the complex meander line structure can be treated as a simple transmission line

element, which provides a scalable solution. Finally, the presented unit cell model of the meander delay line is expected to be helpful for modern high-speed circuit board designers.

REFERENCES

[1] H. Lee and J. Kim, "Modified Yee's cell for finite-difference time-domain modeling of periodic boundary guiding structure," in *Proc. IEEE MTT-S Int. Microwave Symp. Dig.*, vol. 2, May 2001, pp. 889–892.

[2] A. C. Cangellaris, M. Gribbons, and G. Sohos, "A hybrid spectral/FDTD method for the electromagnetic analysis of guided waves in periodic structures," *IEEE Microwaves Guided Wave Lett.*, vol. 3, pp. 375–377, Oct. 1993.

[3] M. Celuch-Marcysiak and W. K. Gwarek, "Spatially looped algorithms for time-domain analysis of periodic structures," *IEEE Trans. Microwave Theory Tech.*, vol. 39, pp. 860–865, Apr. 1995.

[4] B. J. Rubin and B. Singh, "Study of meander line delay in circuit boards," *IEEE Trans. Microwave Theory Tech.*, vol. 48, pp. 1452–1460, Sept. 2000.

[5] W. P. Harokopus, Jr. and L. P. B. Katehi, "Electromagnetic coupling and radiation loss considerations in microstrip (M)MIC design," *IEEE Trans. Microwave Theory Tech.*, vol. 39, pp. 413–421, Mar. 1991.

[6] B. Archambeault, A. Roden, and O. M. Ramahi, "Using PEEC and FDTD to solve the challenge delay line problem," in *Proc. IEEE Int. Symp. Electromag. Compat.*, vol. 2, Aug. 2001, pp. 827–832.

[7] O. M. Ramahi, "FDTD analysis of conventional and novel delay lines," in *Proc. IEEE Antennas Propagat. Soc. Int. Symp. Dig.*, vol. 4, 2000, pp. 1994–1997.

[8] R.-B. Wu and F.-L. Chao, "Laddering wave in serpentine delay line," *IEEE Trans. Comp., Packag., Manufact. Technol. B*, vol. 18, pp. 644–650, Nov. 1995.

[9] R. E. Collin, *Foundation of Microwave Engineering*, 2nd ed. New York: McGraw-Hill, 1992, ch. 8.

[10] V. Rizzoli and A. Lipparini, "Bloch-wave analysis of stripline- and microstrip-array slow-wave structures," *IEEE Trans. Microwave Theory Tech.*, vol. MTT-29, pp. 143–150, Feb. 1981.

[11] P. Petre and M. Swaminathan, "Spectral domain technique using surface wave excitation for the analysis of interconnects," *IEEE Trans. Microwave Theory Tech.*, vol. 42, pp. 1744–1749, Sept. 1994.

[12] S. B. Worm and R. Pregla, "Hybrid mode analysis of arbitrarily shaped planar microwave structures by the method of lines," *IEEE Trans. Microwave Theory Tech.*, vol. MTT-32, pp. 191–196, Feb. 1984.

[13] E. Takagi, "Frequency dependence of Bloch impedance in a periodic transmission line structure," in *IEEE MTT-S Int. Microwave Symp. Dig.*, vol. 2, May 2001, pp. 779–782.

Heeseok Lee received the B.S. degree in electronic communication engineering from Hanyang University, Seoul, Korea, in 1996 and the M.S. degre from the Korea Advanced Institute of Science and Technology (KAIST), Taejon, in 1998, where he is currently pursuing the Ph.D. degree.

Since 1996, he has been with the Terahertz Media and System Laboratory, Electrical Engineering Department, KAIST, involved with the development of terahertz imaging system and the FDTD modeling of the high-speed digital interconnection.

Mr. Lee received a Scholarship Award from the Korea Foundation for Advanced Studies (KFAS).

Joungho Kim received the B.S. and M.S. degrees in electrical engineering from Seoul National University, Seoul, Korea, in 1984 and 1986, respectively, and the Ph.D. degree in electrical engineering from the University of Michigan, Ann Arbor, in 1993. His doctoral thesis was a study on the femtosecond time-domain optical measurement techniques for the testing of high-speed digital devices and millimeter-wave circuits.

He moved to Picometrix, Inc., Ann Arbor, in 1993, as a Research Engineer, where he was responsible for the development of a picosecond sampling system and a 70-GHz photo-receiver. In 1994, he joined the Memory Division, Samsung Electronics, Kiheung, Korea, where he was engaged in a 1-Gb DRAM design. In 1996, he moved to the Korea Advanced Institute of Science and Technology (KAIST), Taejon. He is currently an Associate Professor with the Electrical Engineering and Computer Science Department, KAIST. Since joining KAIST, his research interests have centered on the modeling, the design and the testing of high-speed interconnections, packages, and connectors over GHz frequency range. Related research topics are signal integrity, crosstalk, SSN, and EMI problems. He also has developed a novel picosecond/THz near-field imaging system by using ultrafast optoelectronic technique for the high-frequency characterization of the interconnections. He is currently on sabbatical leave during the academic year from 2001 to 2002 at Silicon Image, Inc., Sunnyvale, CA, as a Staff Engineer. He has authored or co-authored over 100 technical articles and numerous patents.